ELSEVIER

Contents lists available at ScienceDirect

Applied Ocean Research

journal homepage: www.elsevier.com/locate/apor



Research paper

Development and verification of real-time hybrid model test delay compensation method for monopile-type offshore wind turbines

Wei Shi a,b,*, Jie Fu a, Zhengru Ren c, Madjid Karimirad d, Huimeng Zhou e, Xin Li b,f

- a DeepWater Engineering Research Centre, Dalian University of Technology, China
- ^b Ningbo Institute of Dalian University of Technology, Ningbo, Zhejiang, 315000, China
- ^c Institute for Ocean Engineering, Shenzhen International Graduate School, Shenzhen, 518055, China
- ^d Civil Engineering, School of Natural and Built Environment, Queen's University Belfast, United Kingdom
- e Engineering Seismic Research Center, GuangZhou University, Guangzhou, 510006, China
- f Key Laboratory of Coastal and Offshore Engineering, Dalian University of Technology, China

ARTICLE INFO

Keywords: Monopile-type offshore wind turbines Real-time hybrid model test Delay compensation Force control Test accuracy

ABSTRACT

The real-time hybrid model (RTHM) test is adept at addressing the scale contradiction, the lack of fidelity in wind modelling in hydrodynamic testing facilities and spatial constraints inherent in conventional monopile-type offshore wind turbine (OWT) model testing methods, thus emerging as an effective avenue for conducting physical model tests of Monopile-type OWTs. This method entails the reproduction of aerodynamic loads or platform motions using loading device or vibration tables. Time delays in the physical attributes of the loading device and signal transmission processes within the system can result in error accumulation, with the potential to impact overall system stability. Moreover, time delay compensation algorithms for hybrid model test systems with force control loading can easily generate excessive noise, leading to system divergence. As a result, time delay has emerged as a technical challenge in the RTHM test. To address this issue, this paper has developed second-order and third-order polynomial extrapolation algorithms, alongside an adaptive compensation algorithm. The adaptive compensation algorithm employs the least squares method to identify parameters of the loading system, enabling it to address variations in the time delay of the experimental system caused by the nonlinearity of the loading system and changes in the physical properties of the model. The feasibility and effects of time delay compensation for various algorithms are validated through numerical simulation. Results indicate that the adaptive compensation algorithm surpasses second and third-order polynomial extrapolation compensation algorithms in terms of accuracy and compensation effectiveness. To validate the applicability of the adaptive compensation algorithm, a RTHM test was conducted. Across rotor thrust force (RotThrust) and tower top displacement, there was an average reduction of approximately 5 % and 9 % in the maximum and minimum synchronization errors, respectively. This highlights the efficacy of the delay compensation algorithm in practical applications, notably diminishing time delay errors within the experimental system. The adaptive compensation algorithm continuously adjusts and updates parameters, enhancing the adaptability of the compensation process to time-varying systems.

1. Introduction

The depletion of fossil fuels has prompted an increasing number of countries to adopt policies supporting clean energy alternatives (Smith et al., 2015; Musial et al., 2016; Ren et al., 2023; Shi, et al., 2024), particularly offshore wind power. To investigate the dynamic response of offshore wind turbine (OWT) in intricate environments (Zhang et al., 2022; Shi et al., 2023), the method of physical model testing (Feng and

Shen, 2017; Ren et al., 2024) assumes a pivotal role during the design phase of OWT (Zhang et al., 2024; Ferčák et al., 2022). Nevertheless, challenges arise in traditional model testing due to the distinct scaling laws governing the wind turbine (Perveen et al., 2014) and the platform of OWT. These challenges encompass issues such as scale contradictions (Chen et al., 2024), accurate reproduction of turbulent wind loads, and spatial limitations. The redesign of the blade, guided by criteria such as shape matching, performance matching, and thrust matching (Zeng

^{*} Corresponding author at: DeepWater Engineering Research Centre, Dalian University of Technology, China. *E-mail address:* weishi@dlut.edu.cn (W. Shi).

et al., 2021), falls short of facilitating an in-depth exploration of the fully coupled mechanism of OWTs. This limitation hinders the comprehensive assessment (Wan et al., 2024) of the performance of the OWTs structure (Zhao et al., 2018), presenting a challenging task. The RTHM tests employs a hardware-in-the-loop (HIL) strategy (Shi et al., 2023), utilizing loading devices or vibration tables to replicate wind loads or platform movements. This approach applies computer simulation results to the physical model. Through the utilization of sensors and data transmission systems, the outcomes of numerical and real models undergo cross iteration, fulfilling the requisites for studying the fully coupled mechanism of the experimental object. The hybrid model test method effectively addresses the challenges encountered in traditional model experiments, leading to enhanced efficiency and accuracy.

Despite the substantial advantages of RTHM test (Fu et al., 2023), it is crucial to acknowledge that the loading device must experience time delays in receiving and executing commands due to its physical properties. Furthermore, signal delays may arise during the transmission and exchange of data in the experimental system. The time delay not only influences test accuracy but also jeopardizes the stability of the test under specific conditions, posing a safety risk to both the test device and system. To tackle the challenges arising from time delays, it is imperative to implement compensation for the complete time delay of the experimental system during an RTHM test.

For the first time, Nakashima et al. (2018) conducted a RTHM test. By using the damper located at the base of a multi-story building as the test subject, seismic response test was conducted. The speed-related structural characteristics were tested in the test, thereby enhancing the accuracy of the test results. In 1999, Horiuchi et al. (1999) proposed a solution for the significant issue of RTHM test delay compensation, by utilizing Lagrange polynomial extrapolation to predict the simulation outcomes of the next time step. This process compensates for the delay introduced by the loading device itself. Darby et al. (2002) conducted comprehensive studies on this issue. A compensation algorithm for the adaptive estimation of time delay has been proposed, which effectively addresses the issue of compensation accuracy once the stiffness of the specimen enters the nonlinear stage. A novel model-based servo-hydraulic tracking control method, incorporating feedforward-feedback links, was proposed by Phillips and Spencer (2011) for displacement control in hybrid test systems, to achieve real-time and accurate tracking of desired displacements. Chae et al. (2013) effectively enhanced actuator control precision by incorporating the nonlinearity of the combined system through online updating of the coefficients of the system transfer function. An almost precise compensation scheme was proposed by Wu et al. (2013) to address prediction inaccuracies and uncertainty in delay estimation. In this scheme, displacement was compensated for using an upper-bound delay, and the desired displacement was determined through an optimization process. Palacio-Betancur and Soto (2019) utilized the principles of the Adaptive Time Series Compensator (ATSC) and employed the Recursive Least Squares (RLS) algorithm for estimating controller parameters to reduce computational efforts in simulations. Ning et al. (2023) proposed a model-based adaptive feedforward-feedback control method considering an additive error model, which effectively enhances the accuracy and stability of RTHS, while significantly reducing reliance on adaptive control laws. The aforementioned algorithms have been applied in displacement compensation for hybrid model tests in the field of civil engineering, but their application in force-controlled loading systems requires further validation. Chae et al. (2018) proposed a novel real-time force control method using an ATSC and compliant springs to address the application issue of compensation algorithms in force-controlled loading systems.

Hall et al. (2018) considered the simulation time and communication efficiency of the numerical substructure. Numerical substructure refers to the simulation model, which usually divides the parts of the structure that are easy to solve and have clear response patterns into numerical substructures. Extrapolation time-delay compensation algorithm is used to compensate for the actuator delay. The loading device's delayed

response results in a time delay (Chabaud et al., 2013), introducing false energy into the system, which has the potential to cause instability (Cao and Tahchiev, 2013). Sauder et al. (2016) holds the same viewpoint and has verified the changes in energy. The fixed forward prediction method was employed (Bachynski et al., 2016), which is based on a delay compensation strategy predicted by kinematics (Berthelsen et al., 2016). This method assumes the existence of a constant delay between the measurement position and the applied force, which is determined through testing. By conducting a free decay test, applicability of compensation algorithm is verified to ensure there is no inadvertent alteration in the system energy. Vilsen et al. (2019) have developed a uniform method for predicting and compensating for time delays resulting from measurement systems (Vilsen et al., 2018), communication, calculation time, and the inherent properties of the actuator (Vilsen et al., 2017). This method predicts the position and velocity values in the next time step by performing third-order polynomial extrapolation using the first 6 data points. The advantage is that it can compensate for system delay and avoid introducing unacceptable noise. To address the issue of time-delay, Azcona et al. (2019) takes the approach of calculating the outcomes of the subsequent time step in advance, (Azcona et al., 2014) and subsequently, updating the aerodynamic thrust when transmitting the measured motion response of the physical substructure to the numerical substructure for computation. Physical substructure refers to the physical model, which usually divides the complex reaction patterns in the structure that are difficult to accurately simulate into physical substructures.

The aforementioned experts and scholars have contributed significantly to the advancement of RTHM test and its application in OWTs. The time delay algorithms employed are all polynomial interpolation methods, and there has been no quantitative examination of the performance of these time delay algorithms. There is a lack of comprehensive research on the properties of various algorithms and their applicability within the realm of Monopile-type OWTs. This paper examines the frequently employed extrapolation polynomial algorithm and presents an adaptable time delay compensation technique that is founded on the online estimated of discrete model parameters of the loading system for Monopile-type OWT. This technology updates model parameters through the least square method with a forgetting factor, and the compensation command of the actuator is generated using the desired force, the measured force, and the previous force command. The feasibility and effects of time delay compensation for second-order, third-order polynomial extrapolation and adaptive algorithm are verified through numerical simulation. The Monopile-type OWT's RTHM test is also conducted to verify the practical application effect of the algorithm. This test developed the AeroDyn as numerical substructure, added the adaptive time delay compensation algorithm, and then designed a physical substructure to reproduce the air load using a rod actuator. The feasibility and accuracy of the adaptive time delay compensation algorithm are verified. The experimental results demonstrate that the adaptive time delay compensation algorithm effectively reduces the maximum and minimum synchronization errors of approximately 5 % and 9 % of RotThrust and tower top displacement.

The remainder of this paper is organized as follows. Section 2 describes the principles of various time delay compensation algorithms in RTHM test. Section 3 presents the simulation implementation of this method. To validate the efficiency of the time delay compensation algorithm, the experiment settings for the algorithm were detailed in Section 4. Section 5 discusses the performance of time delay compensation algorithms under various operating conditions. Section 6 discusses the compensation algorithm's conclusion.

2. Time delay compensation algorithm

In real-time hybrid model testing, the loading device must accurately and timely apply loads to the physical substructure and feedback the physical substructure's responses to the numerical substructure. However, during the testing process, runtime is required for numerical substructure calculations, and response delays in the loading device are inevitable due to its physical characteristics. It is assumed that the expected force f_{i+1} at a time t_{i+1} is obtained by calculation at time t_i . If the system time delay exceeds the simulation calculation time interval Δt , the command issued at time t_i needs to be corrected to apply force f_{i+1} to the test piece at time t_{i+1} . The method used to correct the command is referred to as time delay compensation. If the dynamic characteristics of the system, such as the transfer function, are known, then the force command can be determined by the intended force required to achieve the desired compensation. This paper presents two distinct compensation methods for the RTHM test system of Monopile-type OWTs, namely a compensation method rooted in polynomial extrapolation and an adaptable time-delay compensation method.

2.1. Compensation method based on polynomial extrapolation

Horiuchi et al. (1999) first proposed the polynomial extrapolation time-delay compensation method, which is currently the most frequently employed time-delay compensation method in RTHM test. This method assumes that the time-history curve of the displacement of the specimen driven by the actuator is a polynomial function with time as the independent variable. Select the currently known displacement data at time and the expected displacement d_{i+1} at the next integration time t_{i+1} to determine the displacement time history curve of the model, which adopts the Lagrange interpolation method. Use this polynomial curve to extrapolate to calculate the displacement $d(t_{i+\tau})$ at the time $t_{i+\tau}$, and issue this command at time t_i . If the command of displacement $d(t_{i+\tau})$ is kept unchanged in the interval $(t_i, t_{i+\tau})$, it can be seen from the definition of time delay that $d(t_{i+\tau})$ must be realized at $t_{i+\tau}$, so that the x-degree polynomial trajectory curve of the specimen must reach the desired displacement d_{i+1} at time $t_{i+\tau}$. Usually, the other n -1 data besides the displacement d_{i+1} can also be taken as the expected displacement, to make the fitted polynomial curve smoother. Therefore, this paper employs the Lagrange extrapolation method to compare the second-order and third-order polynomial extrapolation time-delay compensation methods, which have a broad range of applications. The second-order compensation algorithm's expression is as follows (Bonnet

$$f_c(t_i) = \widetilde{f}(t_i + \tau) = a_0 f_i + a_1 f_{i-1} + a_2 f_{i-2}$$
(1)

where $a_0 = 1 + \frac{3}{2}\eta + \frac{1}{2}\eta^2$, $a_1 = -(2\eta + \eta^2)$, $a_2 = \frac{1}{2}\eta + \frac{1}{2}\eta^2$, $\eta = \frac{\tau}{\Lambda r}$.

The third-order compensation algorithm's expression is as follows (Bonnet et al., 2007):

$$f_c(t_i) = \widetilde{f}(t_i + \tau) = a_0 f_i + a_1 f_{i-1} + a_2 f_{i-2} + a_3 f_{i-3}$$
(2)

where
$$a_0=1+\frac{11}{6}\eta+\eta^2+\frac{1}{6}\eta^3, a_1=-\left(3\eta+\frac{5}{2}\eta^2+\frac{1}{2}\eta^3\right), a_2=\frac{3}{2}\eta+2\eta^2+\frac{1}{2}\eta^3, a_3=-\left(\frac{1}{3}\eta+\frac{1}{2}\eta^2+\frac{1}{6}\eta^3\right), \eta=\frac{\tau}{\Delta t}$$
 where a_i is the coefficients; η is the parameter; τ is the time delay; Δt the time interval; t_i is the time of the i-th step; \widetilde{f} is the predictive force; f_c is the command force; f is the

2.2. Adaptive time delay compensation method

expected force.

The proposed time-delay compensation methods above assume that the system delay is constant. Due to the nonlinear characteristics of the test model and servo loading system, the system time delay often changes during the RTHM test. The adaptive control method can adapt to the time-varying characteristics of the controlled object by identifying the system model and adjusting the corresponding controller. Therefore, this paper incorporates the fundamental principle of adaptive4 control to achieve adaptable compensation for the time delay of the loading

system in the RTHM test of Monopile-type OWT (Rui and Zongji, 2009). The working principle is shown in Fig. 1.

The system model establishes the relationship between the input and output of the test loading system. After estimating the unknown parameters of the model, it is possible to predict the response of the loading system to the specified command based on this foundation. The time delay of the loading system is a characteristic of the system. Hence, identifying the system parameters can effectively capture the change in the time delay. The system discrete model can be established as follows:

$$f_{c}^{i} = \sum_{i=1}^{p} f_{c}^{i-j} \cdot \theta_{c}^{j} + \sum_{k=1}^{q} f_{m}^{i+1-k} \cdot \theta_{m}^{k}$$
(3)

where f_c is the command force of loading system; f_m is the measured force of the loading system; θ_c^j, θ_m^k is the corresponding loading system parameter.

Written in matrix form, that is:

$$f_c^i = \varphi_i^T \theta \tag{4}$$

with

$$\varphi_i^T = \left[f_c^{i-1}, \dots, f_c^{i-p}, f_m^i, f_m^{i-1}, \dots, f_m^{i-q} \right]$$
 (5)

$$\theta = \left[\theta_1^c, \dots, \theta_p^c, \theta_1^m, \dots \theta_q^m\right]^T \tag{6}$$

where θ is the set of corresponding loading system parameter; φ_i^T is the set of forces in the loading system; p,q denoting the numbers of parameters

To track the change of system characteristics in real-time after simplifying the test system to a discrete model, it is necessary to estimate the parameter θ_c^j in formula (3) online during the test. In this study, we employ the recursive least squares algorithm with a forgetting factor (Pang and Cui, 2009) to estimate parameters. With its small storage capacity and simple calculation, this algorithm can effectively overcome the phenomenon of "data saturation". The algorithm can be expressed as:

$$\widehat{\theta}_{i} = \widehat{\theta}_{i-1} + \frac{P_{i-1}\varphi(i)}{\lambda + \varphi_{i}^{T}p_{i-1}\varphi_{i}} \left(f_{c}^{i} - \varphi_{i}^{T}\widehat{\theta}_{i-1} \right)$$

$$(7)$$

$$P_{i} = \frac{1}{\lambda} \left(I - \frac{P_{i-1} \varphi_{i}}{\lambda + \varphi_{i}^{T} P_{i-1} \varphi_{i}} \varphi_{i}^{T} \right) P_{i-1}$$

$$\tag{8}$$

where λ is the forgetting factor such that $0.9 \le \lambda \le 1$; *I*is an identity matrix. P_i is the covariance matrix at the i-th step, and $\hat{\theta}_i$ represents the identified parameters at the i-th step, the starting value P_0 and $\hat{\theta}_0$ are calculated using the relevant data obtained by the early off-line test, and the specific algorithm is (Wang et al., 2020):

$$\widehat{\theta}_0 = \left(\Phi^T \Phi\right)^{-1} \Phi^T Y \tag{9}$$

$$P_0 = \left(\Phi^T \Phi\right)^{-1} \tag{10}$$

$$\Phi = \left[\varphi_1, \varphi_2, \cdots, \varphi_L\right]^T, Y = \left[f_c^1, f_c^2, \cdots, f_c^L\right]^T$$
(11)

where L indicates the length of the data; Φ is the measured of load the system; Y is the command of load the system. The $\widehat{\theta}_0$ obtained by this algorithm is quite satisfactory for meeting the test requirements. However, testing or simulation is necessary to fully consider the frequency components of sufficient offline signals in the initial stage of the system. Failure to do so may result in excessive errors in the estimated starting value, thereby compromising the accuracy and safety of the test. The structural reaction obtained through numerical simulation can also serve as the anticipated force for carrying out the preliminary parameter estimated test.

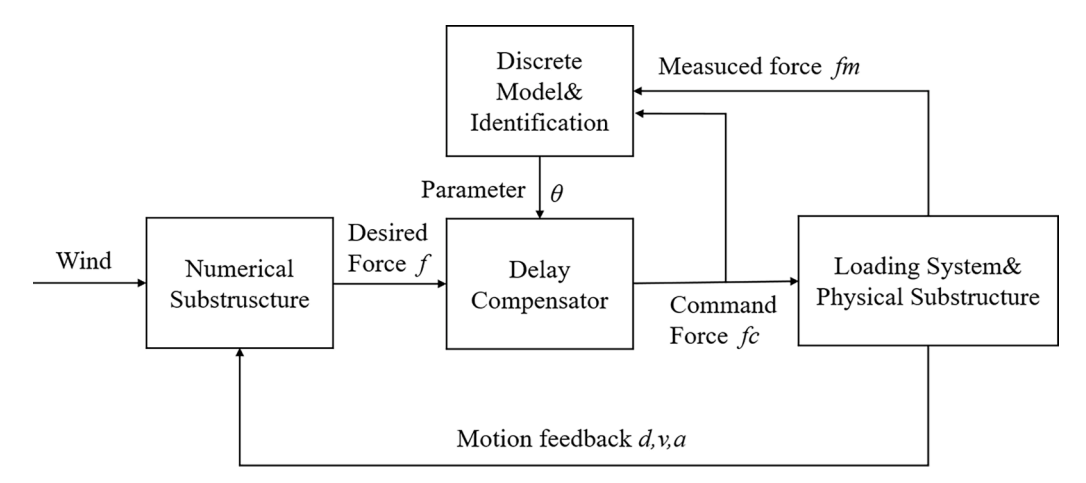


Fig. 1. Principle of adaptive delay compensation for the RTHM test of Monopile-type OWT.

During the test, the parameters estimated by formulas (7) and (8) can directly and effectively reflect the current state of the servo system, including the characteristics of system delay. The system command is calculated based on the inverse model of the discrete model. Due to its ability to automatically track changes in system time delay and its adaptive characteristics, this method is referred to as the adaptive time delay compensation method in this paper. The method is as follows:

First, at the time t_{i+1} , the system model of formulas (4) and (5) can be expressed as:

$$f_{c}^{i+1} = \varphi_{i+1}^T \theta_{i+1} \tag{12}$$

$$\varphi_{i+1}^{T} = \left[f_c^i, \dots, f_c^{i-p+1}, f_m^{i+1}, f_m^i, \dots, f_m^{i-q+1} \right]^T$$
(13)

Assuming that the model parameters do not change much in $t_i - t_{i+1}$, the model parameter $\hat{\theta}_i$ estimated in the *i*-th step can be used to approximate θ_{i+1} , that is:

$$\theta_{i+1} \approx \widehat{\theta}_i$$
 (14)

At this moment, in formula (13), f_m^{i+1} is unknown, $f_c^i, \cdots, f_c^{i-p+1}, f_m^{i-1}, f_m^{i-2}, \cdots f_m^{i-q+1}$ are known. At this time, the desired force f^{i+1} in the test can be calculated by AeroDyn software. The aim of time-delay compensation control is to bring the measured force as close as possible to the desired force (Wang et al., 2020). Therefore, when calculating the command, it can be assumed that:

$$f_{\rm m}^{i+1} = f^{i+1} \tag{15}$$

That is, the compensation method is:

$$f_{\rm c}^{i+1} = \varphi_{i+1}^T \widehat{\theta}_i \tag{16}$$

$$\varphi_{i+1}^{T} = \left[f_c^i, \dots, f_c^{i-p+1}, f_m^{i+1}, f_m^i, \dots, f_m^{i-q+1} \right]^T$$
(17)

At this moment, $\widehat{\theta}_i$ is sufficiently close to the actual model parameter θ_{i+1} , the command force $f_{\rm c}^{i+1}$, obtained from formula (15), is forwarded to the loading system. Consequently, the measured force $f_{\rm m}^{i+1}$ of the test substructure will approximate the expected force $f_{\rm m}^{i+1}$, thereby achieving the desired time delay compensation effect.

3. Numerical simulation

In order to examine the precision of various time delay compensation algorithms, this section evaluates their differences through the development of the AeroDyn program, wherein various algorithms for time delay compensation were integrated. The overall numerical model adopts National Renewable Energy Laboratory (NREL) 5 MW wind

turbine, and variable pitch control is used during simulation. During the subsequent testing process, the system time delay was evaluated, and the initial parameters θ of the system transfer function and time delay compensation algorithm were established based on the system input and output data obtained from the test. By testing the sine curve using an input amplitude of 0.4 N and a frequency of 2 Hz from the test system, it has been determined that the time delay error of the test system is approximately 22 ms, as illustrated in Fig. 2.

A comparison between the command force with delay and the desired force is conducted through simulation. The data in this section are all full-scale data. Set the system time delay to 22 ms, time step to 0.01 s, and simulation duration to 380 s. The TurbSim software generates turbulence wind files based on the Kaimal spectrum as per International Electrotechnical Commission (IEC) standards. Three sets of turbulent wind conditions are established based on wind speeds of 8 m/s (under the rated wind speed), 11.4 m/s (the rated wind speed), and 18 m/s (above the rated wind speed), ensuring that they cover the wind speed conditions experienced by Monopile-type OWTs during operation. As shown in Table 1. As the outcomes of various algorithms do not reveal significant differences in time series, the detailed differences upon closer inspection are presented below. Please refer to the close-up views below for specific views. In order to clearly express the errors between the forces calculated by different algorithms and the expected forces, we divide the two and define the results as correlation errors. The formula is

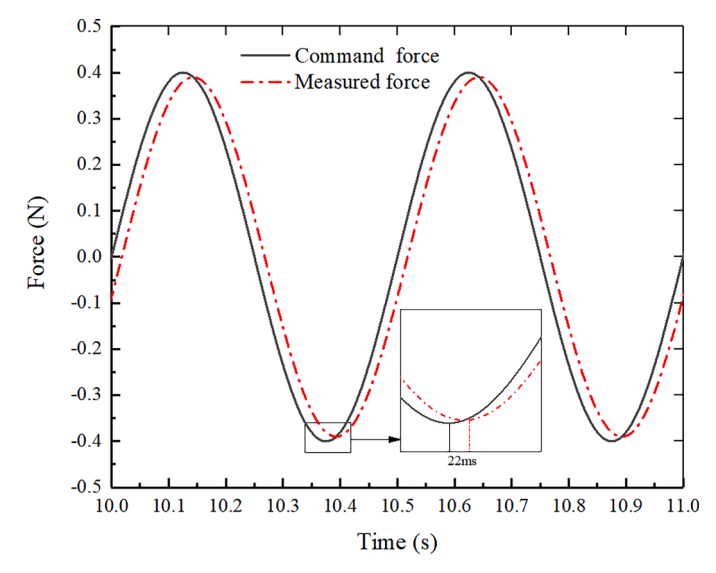


Fig. 2. Amount of time delay.

Table 1
Simulated working conditions setting.

Load case	Um (m/s)	TI (%)	Time-delay compensation arithmetic		
1	8	17	2-Order	3-Order	Adaptive
2	11.4	17	2-Order	3-Order	Adaptive
3	18	17	2-Order	3-Order	Adaptive

as follows:

$$E_c = F_a/F_e \tag{18}$$

where E_c is the correlation errors; F_a is the forces calculated by different algorithms; F_e is the expected forces. The larger the difference in correlation errors, the more significant the error in the corresponding time delay algorithm. The specific view can be observed in the following correlation error chart of time histories.

Figs. 3(a), 4(a), and 5(a) are Close-up views of the time domain results of force differences corresponding to various wind speeds. At wind speeds of 8 m/s and 11.4 m/s. Three algorithms can effectively reduce the cumulative load synchronization error caused by delay compensation, namely the cycle extension error. Under a wind speed of 18 m/s, significant errors were observed between 120 and 170 s. The force error will decrease, indicating that second-order and third-order algorithms will impact the stability of the test. The primary reason is that employing measured force for time delay compensation will amplify the experimental system's noise, leading to a notable vibration of the command force. The second-order and third-order time delay compensation algorithms can be relatively rough, causing small fluctuations, when the experimental system is affected by noise. The adaptive time delay compensation algorithm exhibits a relatively smooth behavior with minimal changes in command values, suggesting a high-quality resistance to noise in its adaptive compensation method.

Figs. 3(b), 4(b), and 5(b) present the time-domain correlation analysis of force differences at various wind speeds. It is evident that the maximum error value at 8 m/s wind speed is about 0.2 %, and the maximum error value at 11.4 m/s wind speed is about 0.5 %. The compensation abilities of the three delay compensation algorithms differ under wind speeds of 18 m/s. The adaptive algorithm excels in compensating for delay error, with a maximum error of approximately 0.5 %, compared to the maximum error of approximately 3 % for the second-order compensation algorithm and approximately 4 % for the

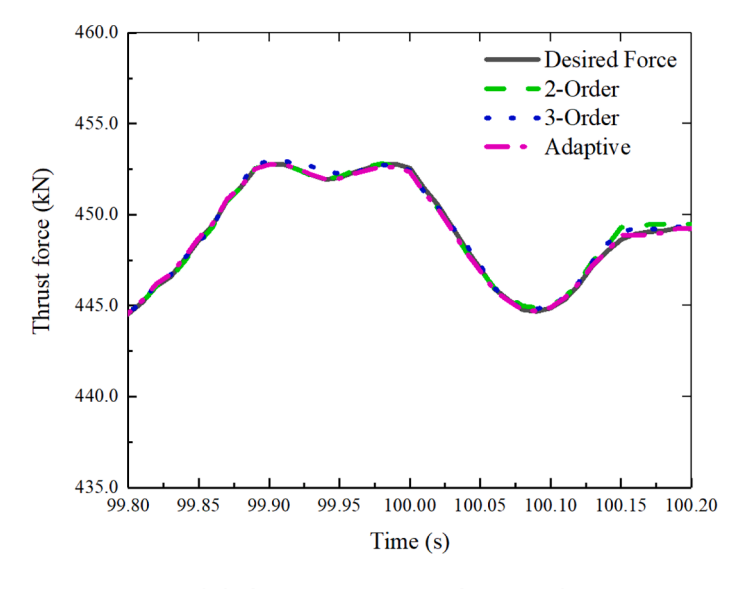
third-order compensation algorithm. The adaptive algorithm exhibits relatively exceptional compensation capabilities. Different time delay algorithms can effectively compensate for time delay under various wind speeds, thereby reducing the phase error between the command force and the expected force.

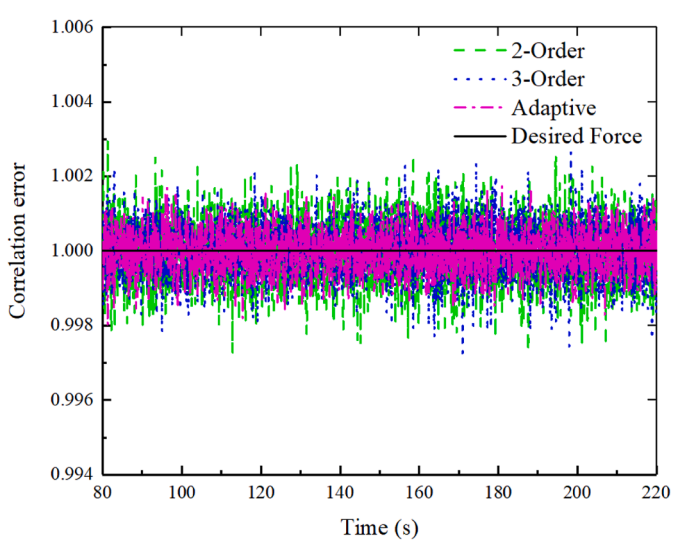
4. Validation tests

4.1. Characteristics of tests

In order to verify the applicability of the algorithm further, a RTHM test was conducted using Monopile-type OWT as the object. The wind turbine is the NREL 5 MW wind turbine proposed by Jonkman et al. (2009). We used a variable pitch control strategy in the testing (Cao et al., 2022), which is a controller included in the FAST software (Zeng et al., 2021). However, to assess the feasibility of Monopile-type OWT RTHM test, variable pitch control was not applied to the wind turbine at rated speeds of 18 m/s. Table 2 displays the fundamental parameters of the turbine, tower, and foundation.

Taking into account the geometric dimensions of the prototype and the laboratory conditions, the scale of the RTHM test is determined to be 1:90 based on the geometric similarity criterion and Froude's similarity law. During the tower design process, this paper has opted to emphasize the realization of crucial tower characteristics that influence the coupling effect between the nacelle and the platform. Specifically, the first-order frequency, along with the tower's height, need to conform to the prototype parameters' scaling requirements to ensure the precision of the entire physical model. Its dimensions and center of mass are redesigned for elasticity and inertial force. The testing strategy for RTHM primarily involves employing numerical substructures and loading devices to reproduce turbulence wind loads. Force commands calculated by the numerical substructures are transmitted to the loading devices, which then act the physical model. The physical model generates motion response under the action of force, which is fed back to the numerical substructure through sensors. This motion response participates in the calculation of aerodynamic loads in numerical substructures, forming a closed-loop data exchange. Through this approach, the coupling effect between aerodynamic loads and the physical model is achieved, it was deemed that the wind turbine and nacelle in this experiment could be replaced with a mass block. Design and manufacture physical substructures based on geometric similarity, and meet the





(a) Close-up view of thrust force

(b)Time histories correlation error

Fig. 3. Comparison of different thrust forces (LC 1).

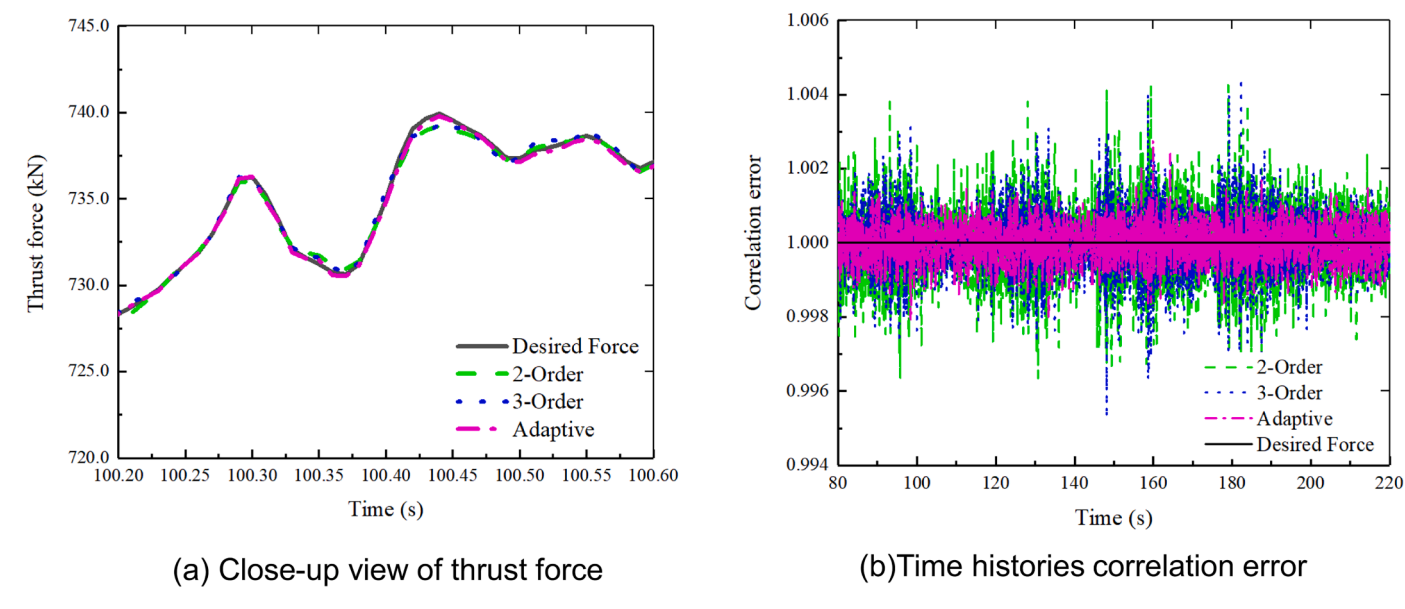


Fig. 4. Comparison of different thrust forces (LC 2).

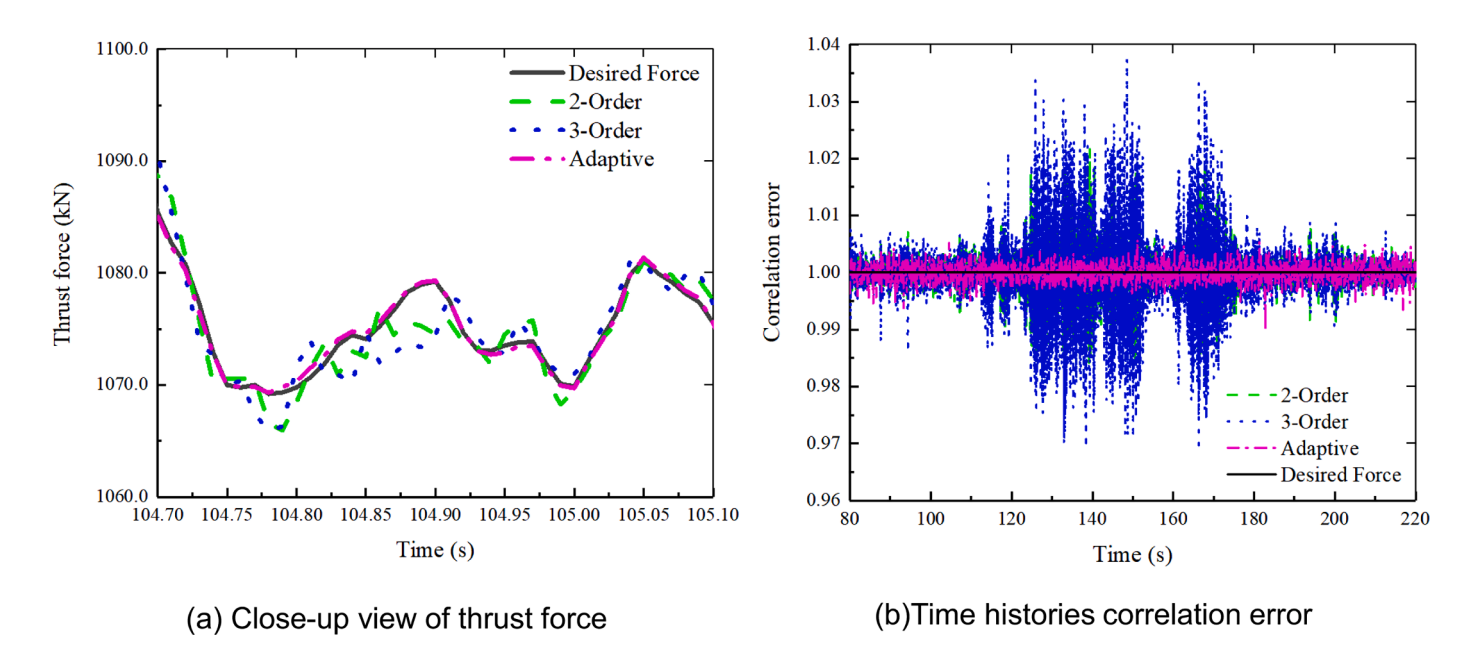


Fig. 5. Comparison of different thrust forces (LC 3).

Table 2Main properties of NREL-5 MW baseline wind turbine (Jonkman et al., 2009).

Parameter	Value		
Rated power	5 MW		
Rotor orientation	Upwind		
Rotor, Hub diameter	126 m, 3 m		
Hub height	90 m		
Cut-in, Rated, Cut-Out Wind speed	3 m/s, 11.4 m/s, 25 m/s		
Cut-in, Rated, Rated Rotor Speed	6.9 rpm, 12.1 rpm		
Overhang, Shaft tilt, Precone	5 m, 5°, 2.5°		
Rotor, Nacelle, Tower mass	110 t, 240 t, 347.46 t		
Tower top diameter, Wall thickness	3.87 m, 0.019 m		

quality requirements after scaling through the strategy of mass replacement Additionally, we have redesignated and manufactured the inner and outer diameter dimensions of the tower as well as the connection flange between the lower part and the foundation platform. In order to match the natural frequency of the tower, an aluminum cylindrical block, appropriately sized and weighted, is devised and placed at the upper end of the tower. Simultaneously, the connection with the tower is designed to be detachable, facilitating the addition of a force sensor to gauge the force at the tower's peak. Fig. 6 shows geometric information and physical drawing of physical model. Table 3 compares each parameter between the test turbine system's design value and the NREL turbine system's target value (The center of mass and moment of inertia are both relative to the sea level position).

In order to verify the accuracy of the physical substructure model of the tower, a cartesian coordinate system is established with the geometric center of the tower base as the coordinate origin, the downwind direction as the X axis, the crosswind direction as the Y axis, and the vertical direction as the Z axis. The physical substructure of the tower's three-dimensional finite element model is established using the finite element software ANSYS, with all components being simulated using the solid element of SOLID 163. Define the tower and turbine mass blocks

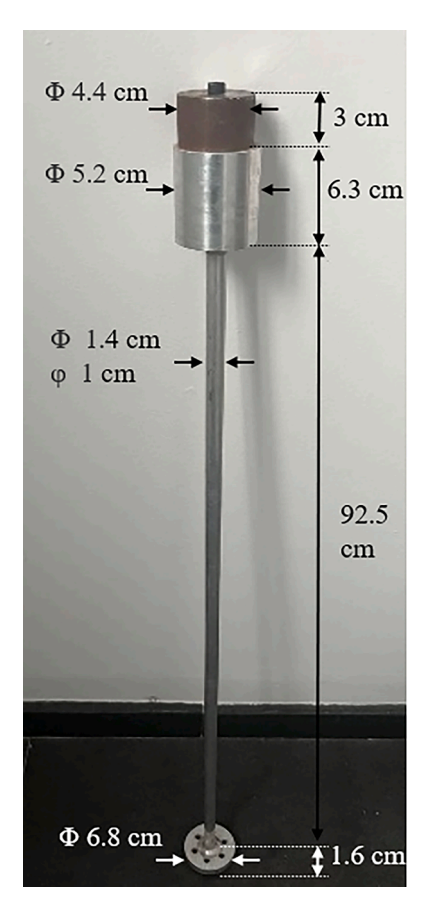


Fig. 6. Geometric information and physical drawing of physical model.

Table 3Comparison of error between model and prototype after scaling.

Parameter	Design value	Target value	Error
Mass	1131.0 g	1143.3 g	-1.06 %
Centroid position	88.4 cm	87.5 cm	1.04 %
Ixx	41441623.27 g*cm ²	42486423.39 g*cm ²	-2.46 %
Iyy	41441623.27 g*cm ²	42158917.68 g*cm ²	-1.70 %
Izz	23624455.43 g*cm ²	24866615.85 g*cm ²	-5.00 %

according to the standard properties of aluminum and iron materials. Constraints were applied at the base of the tower for modal analysis and were compared with the design outcomes.

Based on Table 4, it is evident that the frequency error between the finite element results and the actual model is 3.96 %. The primary reason is that the physical substructure model simplifies the structure of the turbine and nacelle by only retaining the mass, inertia, and other relevant factors, without taking into account the structural configuration of the upper structure. These factors impact the order of the whole model's foundation frequency excitation before and after, in addition to the value of the vibration frequency. Nevertheless, the error remains within an acceptable limit, and essential data like mass, center of mass, and moment of inertia meet the necessary criteria, enabling the

 Table 4

 Comparison of frequency error between model and prototype after scaling.

	Full scale (Hz)	1/90 Scale (Hz)	ANSYS results	Error
Model foundation frequency	0.33	3.15	3.28	3.96 %

utilization of the physical substructure for the RTHM test.

4.2. Test setup

During the RTHM test, the AeroDyn numerical substructure operates within the simulator to evaluate the aerodynamics of the Monopile-type OWT under various operating conditions. The load is calculated in its full scale, then connected to the real-time machine controller through a User Datagram Protocol/Internet Protocol (UDP/IP) communication mechanism, and finally, converted from the full-scale load to a model scale load in accordance with the specified scale. The controller converts the scaled load command into an electrical signal, which is used to drive the actuator and load the physical substructure. The motion response generated by the physical substructure is then returned to the numerical substructure via the sensor. This sensor measures the displacement, velocity, acceleration of the physical model by measuring the rate of change in the length of the rod inside the loading device. Following the feedback on the response results, the numerical substructure calculates the aerodynamics for the subsequent time step based on these results. This ensures that the numerical substructure is fully scale, guaranteeing the consistency between the test results and the real object. Finally, the iterative calculation and closed-loop data of the numerical and physical substructures are formed, reproducing the coupling effect of the Monopile-type OWT system. During the experiment, we measured the motion response of the physical substructure and the force generated by the loading device. All other physical quantities were calculated using numerical substructure methods. The upper computer manages the controller software interface via a Transmission Control Protocol/ Internet Protocol (TCP/IP) communication mechanism, collects and processes data, generates relevant images in real-time, and monitors the loading and response results throughout the test. Fig. 7 portrays the diagram of the RTHM test system.

During the simulation of aerodynamic load (Bachynski et al., 2015), primary consideration (Qin et al., 2023) is given to the horizontal single-degree-of-freedom directional thrust (Zhao et al., 2024). Therefore, to simulate the horizontal thrust of the wind turbine at the hub, this test employs a single-degree-of-freedom actuator. We use an electric actuator, which is loaded by a coreless linear motor and a mechanical linkage, and connected to control software for force control based on Ethernet Control Automation Technology (EtherCAT). This device does

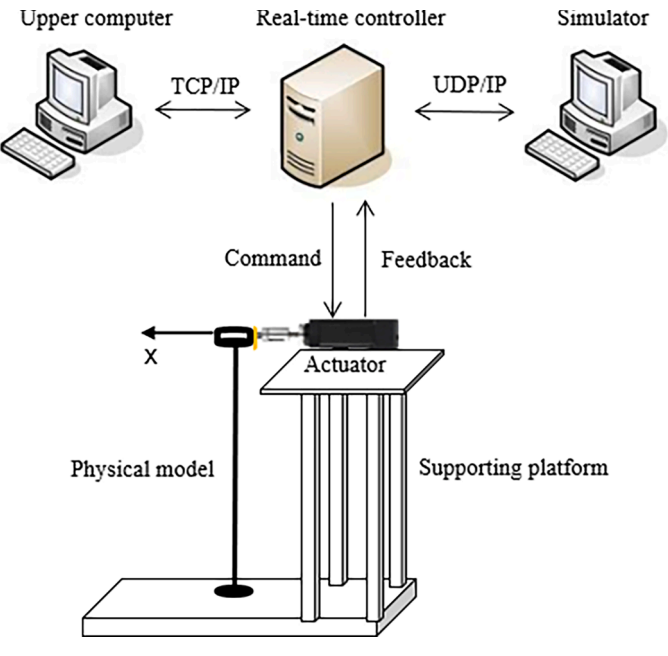


Fig. 7. RTHM test system diagram.

not have traditional mechanical transmission components and is a low-noise driving system. The addition of an air compressor reduces the internal friction of the actuator, thereby minimizing the actual force error. Fig. 8 displays the layout of the RTHM test.

5. Results and discussion

In order to verify the applicability of the proposed adaptive timedelay compensation algorithm in Monopile-type OWTs, the said algorithm was tested. Due to our current research being in the initial stage, we focused on the response characteristics of structures without wave loads, in order to reflect the advantages of real-time hybrid testing and the performance of delay compensation algorithms. Therefore, the current validation test did not consider factors such as waves. Based on the wind speed (Zhai et al., 2024), it can be classified as below the rated wind speed (8 m/s) (Ma et al., 2024), at the rated wind speed (11.4 m/s), or above the rated wind speed (18 m/s). Five sets of turbulent wind conditions are established, encompassing the wind speed conditions of Monopile-type OWTs during operation. Table 5 displays the specifics of the working conditions. Um represents the average wind speed of turbulent wind, TI represents the turbulence intensity of turbulent wind. Turbulent wind parameters were defined according to DNVGL-ST-0437 (DNV G L, 2016). The test suggests that no time delay compensation is being conducted, while Test-Adaptive suggests the incorporation of an adaptive time delay compensation algorithm. OpenFAST is a simulation software that has been developed by NREL (Jonkman and Buhl, 2005). The TurbSim software generates turbulence wind files based on the Kaimal spectrum as per IEC standards (Jonkman, 2014). The test numerical substructure and OpenFAST simulation software make use of the identical turbulence wind file and establish equivalent conditions for blade data, tip and hub loss, in order to carry out RTHM tests.

Three performance indicators are defined to quantify the performance of the adaptive time delay compensation algorithm. The initial indicator, J1, referred to as the maximum synchronization error, is determined by comparing the maximum value of the simulated force with the measured force at the same time step. This measurement aims to elucidate the timing discrepancy between the results and to evaluate the time delay compensation effect of the algorithm. The second indicator, J2, represents the minimum synchronization error, which carries

Table 5
Test conditions.

Load case	Um (m/s)	TI (%)	Test Stra	tegy
1	8	17	Test	Test-Adaptive
2	11.4	17	Test	Test-Adaptive
3	18	17	Test	Test-Adaptive
4	11.4	20.3	Test	Test-Adaptive
5	11.4	14.4	Test	Test-Adaptive

the same connotation as J1, and the comparison yields the minimum value. The normalized root-mean-square error (NRMSE) serves as the definition for the indicator J3, which measures the "average error" of simulation and test results and assesses the degree of data change. Its formula is as follows:

$$J_{3} = \sqrt{\frac{\sum_{i=1}^{N} \left(f^{i} - f_{m}^{i}\right)^{2}}{\sum_{i=1}^{N} \left(f^{i}\right)^{2}}}$$
 (19)

where N represents the length of the data; f_m denote the measurement force at the i-th step; f denote the desired force.

5.1. Performance of algorithm under different wind speeds

By comparing the test results with the rotor thrust force (RotThrust) and tower top displacement of the Monopile-type OWT, which were calculated by the OpenFAST software, the effectiveness of the time-delay compensation algorithm under various wind speeds is validated. Close-up view of RotThrust results were compared, followed by performing power spectral density (PSD) analysis on each of them.

Fig. 9 illustrates the impact of different time delay compensation algorithms on the time-domain results of the rotor thrust force under various operating conditions. To assess the feasibility of Monopile-type OWT RTHM test, variable pitch control was not applied to the wind turbine when operating at speeds exceeding the rated wind speed of 18 m/s. Hence, with an escalating wind speed, the RotThrust experienced by the wind turbine gradually amplifies. This phenomenon is a consequence of OpenFAST's adoption of the Blade Element Momentum (BEM)

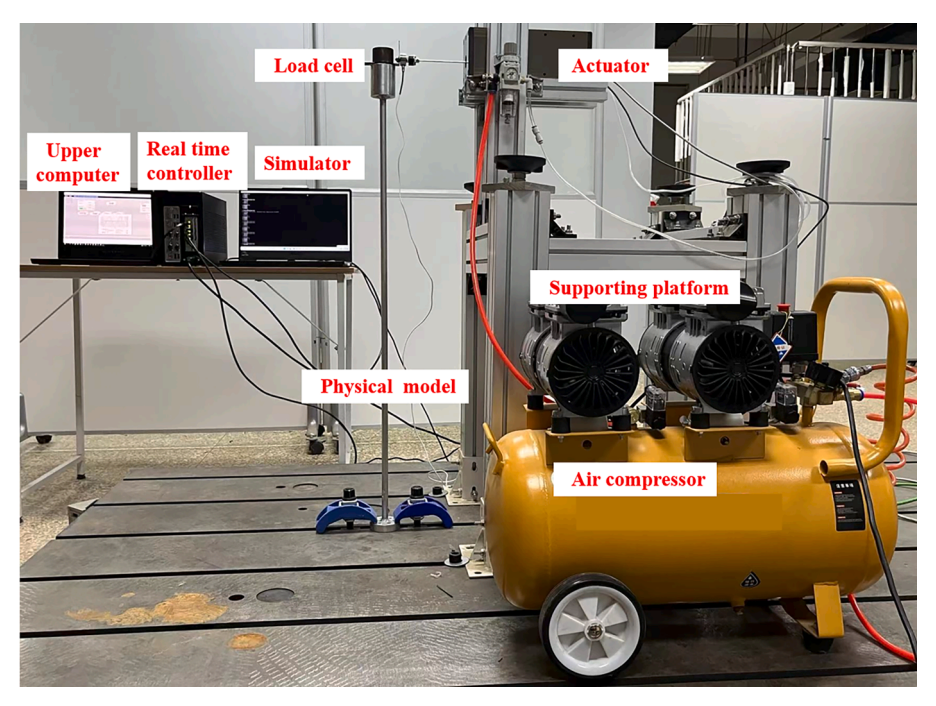
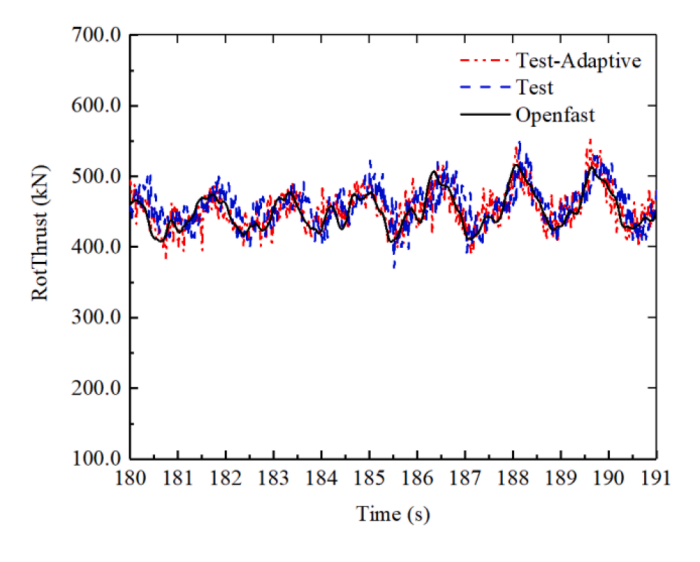
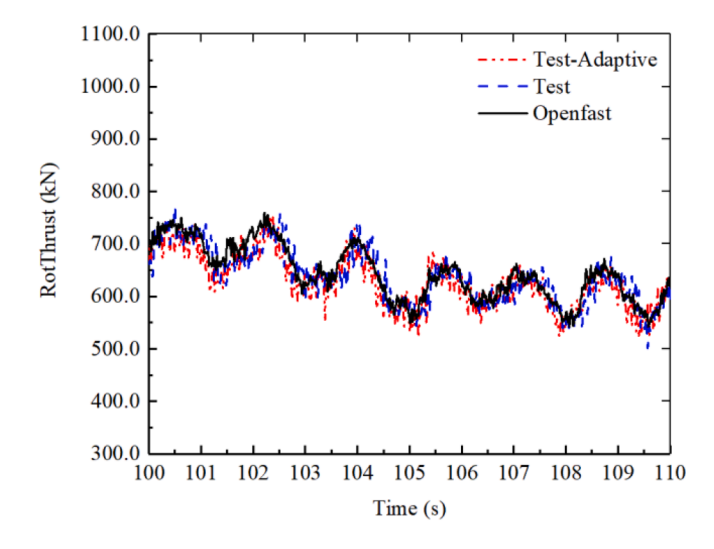


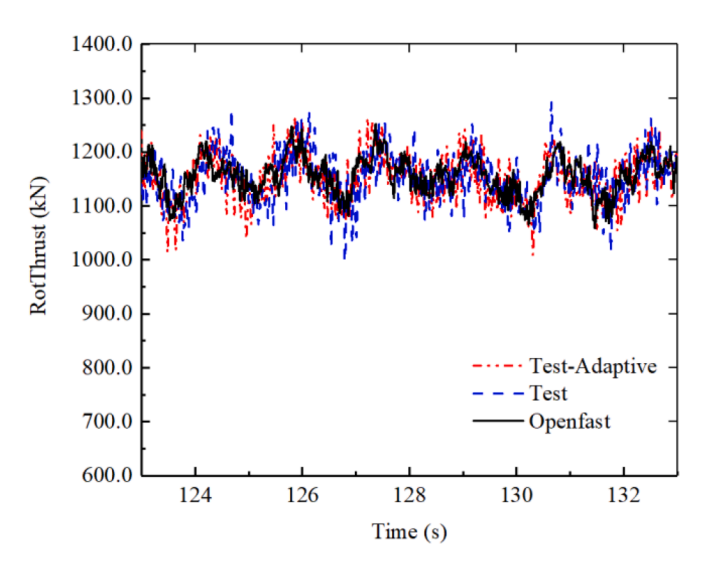
Fig. 8. The layout of the RTHM test.





(a) Close-up view of RotThrust under LC1





(c) Close-up view of RotThrust under LC3

Fig. 9. Comparison of RotThrust results between simulation and test.

calculation theory, which integrates forces acting on individual blade elements along the spanwise direction to yield the forces and moments across the entire blade. Moreover, in experiments without time delay compensation, a lag phenomenon is evident in the RotThrust results. Across diverse operating conditions, the time delay compensation algorithm yields more consistent outcomes between experimentation and simulation. This finding underscores the efficacy of the RTHM test strategy in accurately reproducing turbulent wind loads at the laboratory scale.

Fig. 10 illustrates a frequency domain comparison of the rotor thrust force under different operating conditions. The comparison between experimentation and simulation demonstrates consistency in the low-frequency range, with a relatively prominent frequency peak observed at 0.01 Hz. Analysis indicates that the frequency domain response within this range is notably significant, emphasizing that the frequency energy of turbulent wind is predominantly concentrated in this specific frequency interval. The rotor's 1P frequency appears relatively subtle, whereas the 3P and 6P frequencies manifest more prominently. These aspects warrant consideration during the design phase of Monopile-type OWT to mitigate damage arising from structural resonance. The

inherent frequency of the tower structure remains constant at 0.324 Hz. However, this is not markedly discernible, suggesting that the the rotor thrust force is minimally impacted by the tower structure and is predominantly influenced by the rotor and wind load frequencies. A slight disparity at 1 Hz is noted, attributed to the impact of the fixed framework's fundamental frequency or noise frequency.

Fig. 11 elucidates the influence of time delay compensation algorithms on the time-domain outcomes of tower top displacement under varied operating conditions. At an 8 m/s wind speed, the disparity in RotThrust is relatively modest, leading to a correspondingly restrained tower top displacement under the RotThrust's influence. As the wind speed escalates to 11.4 m/s, the tower top displacement experiences a notable increase. Analogous to the RotThrust, the wind turbine's displacement is more pronounced at an 18 m/s wind speed. However, due to the absence of variable pitch control measures, the RotThrust undergoes a relatively minor change at this wind speed. The tower top displacement is predominantly influenced by wind loads, thus reflecting changes in wind speed.

Fig. 12 elucidates the fluctuations in estimated parameters under diverse operational conditions. In pursuit of a more accurate

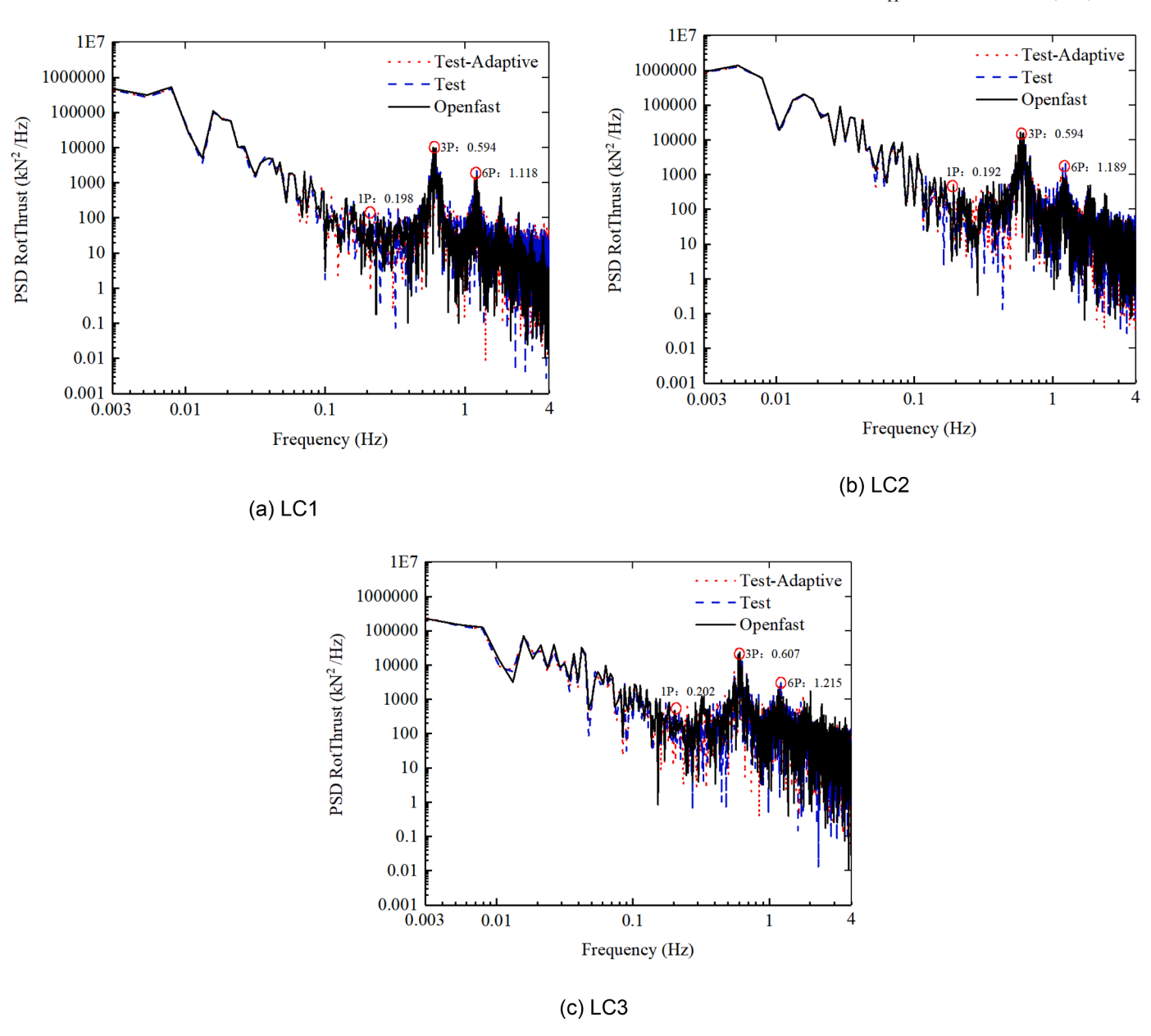


Fig. 10. Comparison of RotThrust PSD results between simulation and test.

reproduction of turbulent wind loads, adjustments are made to the control variables of the loading system itself. Consequently, distinct system parameters are identified for the loading system under varying wind speed conditions. The magnitude of parameter estimation variations under different conditions is relatively small, indicating the stability of the overall time delay in the RTHM test with no significant fluctuations. The fluctuations in estimated parameters result from continuous adjustments and updates by the adaptive algorithm. This ensures that the compensation process adapts more effectively to timevarying systems, achieving a high level of compensation accuracy. In comparison to traditional compensation methods, this approach is particularly suitable for systems with varying time delays. The time delay compensation in the RTHM test performs effectively, successfully reducing test delay errors, illustrating the algorithm's time delay compensation capability and noise resistance.

Table 6 presents the performance indicators of RotThrust and Tower top displacement simulation and testing results obtained under LC 1-3. Examining the RotThrust results, the maximum synchronization error without time delay compensation is 4.68-5.45 %, while the error after

compensation is 1.22-2.12 %. The average minimum synchronization error value without time delay compensation is 9.54-11.25 %, while the error after compensation is 1.97-4.67 %. Examining the results from tower top displacement, the maximum synchronization error without time delay compensation is 8.59-12.88 %, while the error after compensation is 3.63-5.48 %. The average minimum synchronization error value without time delay compensation is 9.79-16.3 %, while the error after compensation is 4.78-6.72 %. Based on the analysis of data results, it can be concluded that the time-delay compensation algorithm effectively reduces the delay error of the test system by comparing J1 and J2 under various wind speeds. There is no positive correlation between various wind speeds and the adaptive time delay compensation algorithms, thus indicating the algorithm's applicability. The root mean squared error of RotThrust results is between 4.39 % and 5.43 %, while the error after compensation is 3.29 % to 4.49 %. Similarly, the root mean squared error of tower top displacement results is between 5.68 % and 7.24 %, with the error after compensation ranging from 4.92 % to 6.59 %. The comparison of J3 under various wind speeds indicates that the time delay compensation algorithm has the potential to minimize the

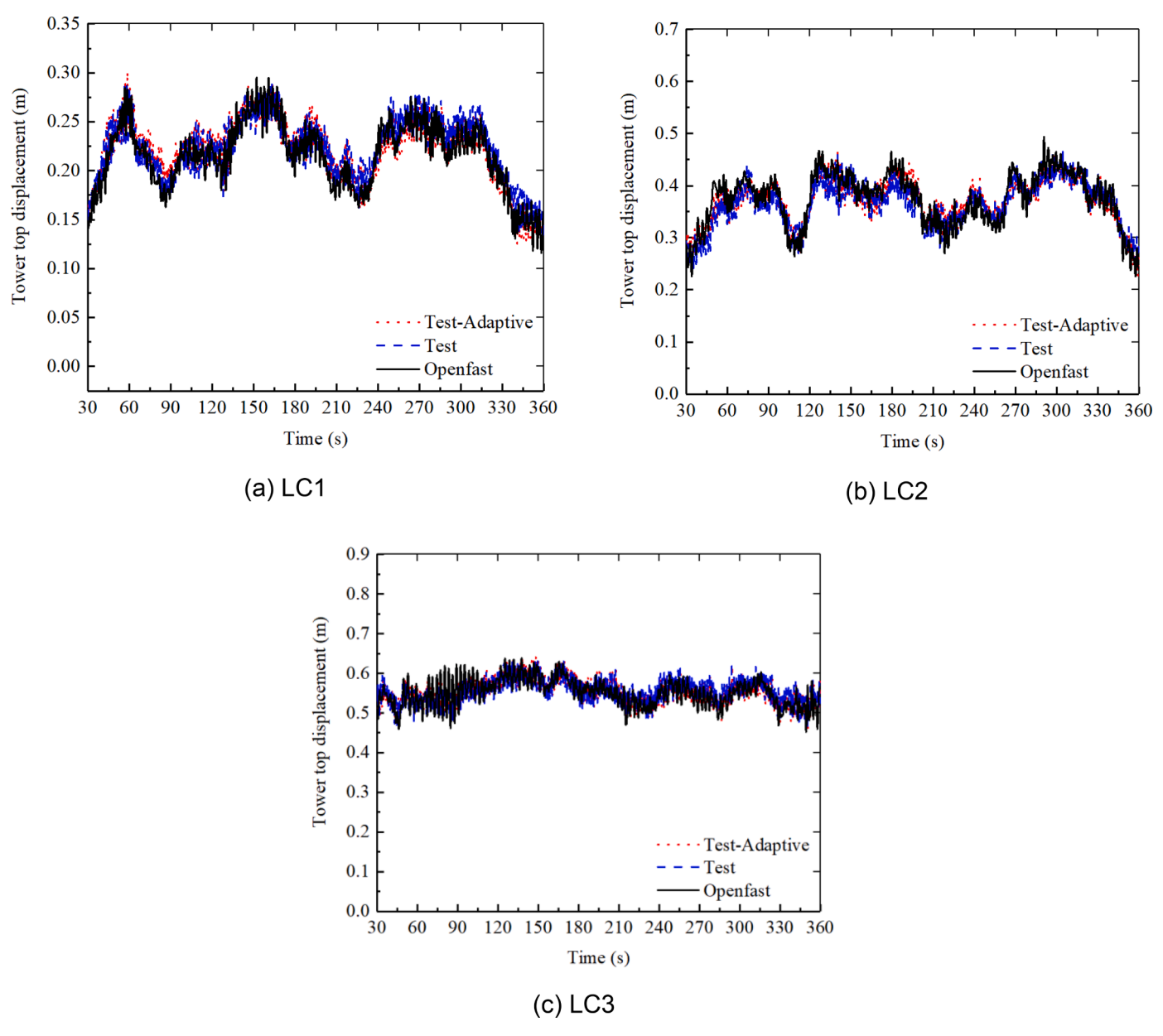


Fig. 11. Comparison of Tower top displacement time domain results between simulation and test.

test system's error, but its effectiveness is constrained by the physical specimens and loading system capabilities, resulting in a less than ideal performance.

Compared with the RotThrust result, the error of the displacement result is larger, because there is a 4 % error in the fundamental frequency of the physical substructure in this test relative to the expected fundamental frequency. This implies that the physical substructure's stiffness is considerably greater than its theoretical value, resulting in displacement outcomes from the experiment being significantly less than those from the simulation. However, the error is within the permissible limit. In experiments with different wind speeds, the results of the experiments and simulations are in agreement, which indicates the superior convenience and scalability of the RTHM test.

5.2. Performance of algorithm under different turbulence intensity

To emphasize the benefits of the RTHM test, the essential parameters were modified in the numerical substructure. Tests were conducted with varying levels of turbulence intensity at a same wind speed. To verify the

performance of the time delay compensation algorithm under various turbulence intensities, compare the RotThrust and tower top displacement results. Because the difference in PSD results was minimal at the same wind speed, only the time domain results were compared.

Figs. 13 and 14 illustrate the impact of the time delay compensation algorithm on the variations in RotThrust and tower top displacement under conditions of the same wind speed but different turbulence intensities. Under identical wind speed conditions, the temporal trends of physical quantities for different turbulence intensities show similarities, albeit with significant distinctions. In contrast to LC4, LC5 exhibits smoother variations in both experimental and simulated time-domain results curves for RotThrust and tower top displacement, resulting in an increased overlap between different curves. The fluctuations in various physical parameters diminish as turbulence intensity decreases. This phenomenon is a consequence of lower turbulence intensities, resulting in a decrease in average wind speed and a reduction in standard deviation.

Fig. 15 depicts the fluctuations in estimated parameters under various operational conditions. Through the parameter estimation

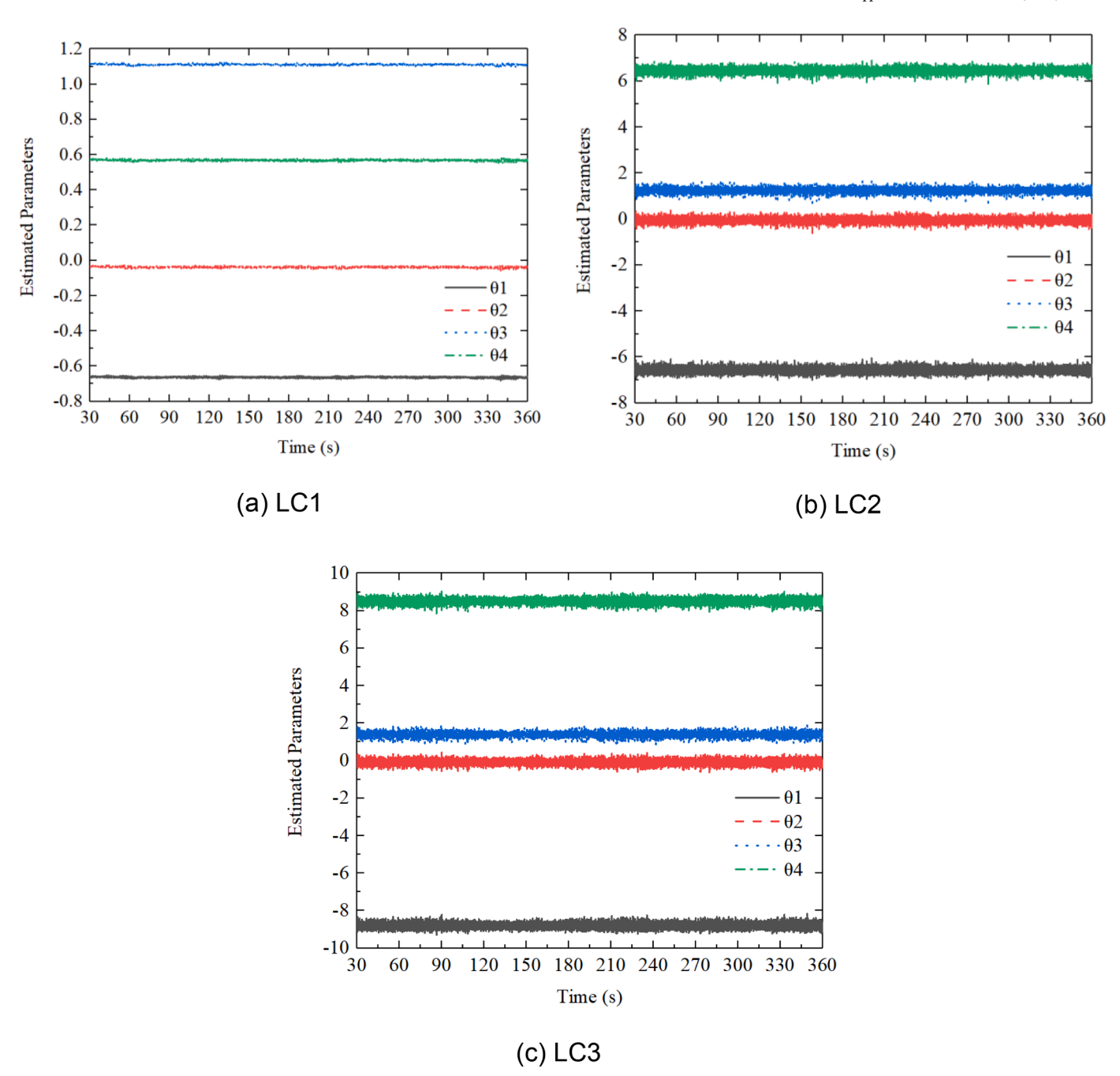


Fig. 12. Estimated parameters of the experimental process.

process employing the integrated adaptive compensation algorithm, the parameters converge to a narrow range of fluctuations. This suggests that alterations in turbulence intensity do not impact the time delay of the loading system. When contrasted with the previous discussion, it becomes apparent that, beyond the control variables of the loading system itself, different turbulence intensities or input commands can exert an influence on the identified system parameters. Furthermore, an analysis of the fluctuations in different physical quantities and parameter estimated outcomes suggests that altering numerical substructure parameters is sufficient for the RTHM test to faithfully reproduce wind loads under diverse turbulence intensities. This underscores the convenience of RTHM test.

Table 7 presents the performance indicators of RotThrust and Tower top displacement simulation and testing results obtained under LC 4-5. Examining the RotThrust results, the maximum synchronization error

without time delay compensation is 5.42-5.61 %, while the error after compensation is 1.68-2.35 %. The average minimum synchronization error value without time delay compensation is 9.79-10.75 %, while the error after compensation is 2.18-2.73 %. Examining the results from tower top displacement, the maximum synchronization error without time delay compensation is 12.43-13.08 %, while the error after compensation is 4.89-5.42 %. The average minimum synchronization error value without time delay compensation is 15.01-15.10 %, while the error after compensation is 5.74-7.29 %. Based on the analysis of data results, it can be concluded that the time-delay compensation algorithm effectively reduces the delay error of the test system by comparing J1 and J2 under various turbulence intensities. The lower the turbulence intensity, the more effective the time delay compensation becomes. The root mean squared error of the RotThrust results is between 4.66 % and 4.67 %, while the error after compensation is 3.25 %

Table 6Performance indicators for RotThrust and Tower top displacement of simulation and test results under different wind speed.

Object	Load case	Test Strategy	J1 (%)	J2(%)	J3 (%)
RotThrust	1	Test	4.68	-11.25	5.43
		Test-	1.22	4.67	4.49
		Adaptive			
	2	Test	5.35	-9.54	4.39
		Test-	2.12	-1.98	3.65
		Adaptive			
	3	Test	5.45	-9.69	3.81
		Test-	1.80	-2.75	3.29
		Adaptive			
Tower top	1	Test	12.88	-16.30	7.24
displacement		Test-	5.40	-6.72	6.59
		Adaptive			
	2	Test	12.51	-14.31	6.48
		Test-	5.48	-6.36	5.64
		Adaptive			
	3	Test	8.59	-9.79	5.68
		Test-	3.63	-4.78	4.92
		Adaptive			

to 3.47 %. Similarly, the root mean squared error of tower top displacement is between 6.80 % and 7.89 %, with the error after compensation ranging from 4.79 % to 6.76 %. The comparison of J3 under various turbulence intensities illustrates that the time delay compensation algorithm can effectively minimize the test system's error.

6. Conclusions

To address the issue of time delay in the RTHM test of Monopile-type OWTs, this paper proposed an adaptive time delay compensation method. This method employs the least squares approach with a forgetting factor to identify and update the loaded system model. Subsequently, the algorithm's applicability and accuracy are substantiated through numerical simulations and RTHM test. The main conclusions are as follows:

(1) The proposed adaptive time delay compensation algorithm generates system force commands using diverse force types, including measured force, expected force, and force from the

- previous time step. The adaptive compensation algorithm has higher compensation accuracy than the second-order and third-order fixed compensation algorithms, and is more suitable for RTHM test of Monopile-type OWTs.
- (2) In diverse operating conditions during the experimental process, through comparative data analysis of different indicators, the delay compensation algorithm can significantly reduce the delay errors in the experimental system. This indicates the effective performance of delay compensation algorithms in practical applications.
- (3) During the experimental process, there is little variation in the estimated parameters under different conditions, indicating the overall stability of the time delay in the entire RTHM test. The adaptive time delay compensation algorithm identifies parameter changes with small magnitudes. This is attributed to the continuous adjustment and updates made by the adaptive algorithm, ensuring the compensation process better adapts to time-varying systems.
- (4) Consistent alignment between simulations and experimental results across varying wind speeds signifies the efficacy of the RTHM test method. This indicates its capability to address challenges encountered in traditional testing and accurately reproduce turbulent wind loads at the laboratory scale.

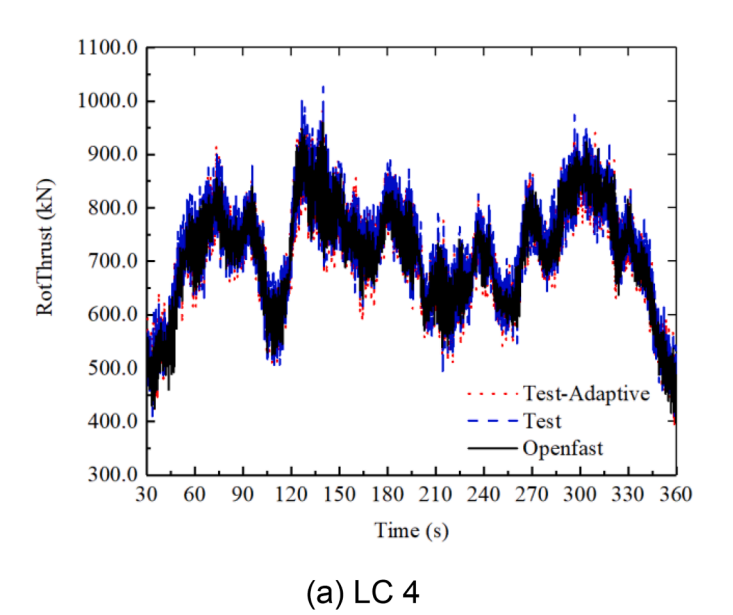
It should be noted that the algorithm employed in this study offers a delay compensation method with high performance for the RTHM test of Monopile-type OWT. However, further study is necessary to investigate the impact of the fundamental frequency of the physical model on the proposed method.

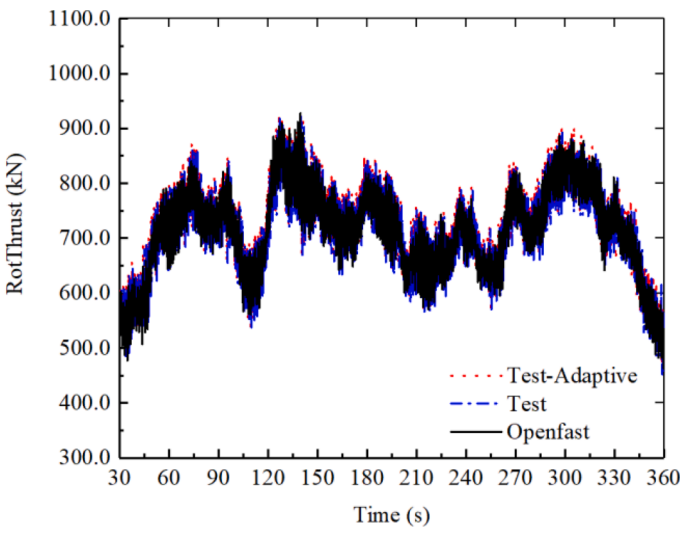
Data access statement

Data are available on request. Due to confidentiality agreements with research collaborators, data supporting this paper can only be made available to researchers subject to a non-disclosure agreement (NDA). Details of the data and how to request access are available by contacting the corresponding authors.

CRediT authorship contribution statement

Wei Shi: Project administration. Jie Fu: Writing – original draft. Zhengru Ren: Supervision. Madjid Karimirad: Writing – review &





(b) LC 5

Fig. 13. Comparison of RotThrust time domain results between simulation and test.

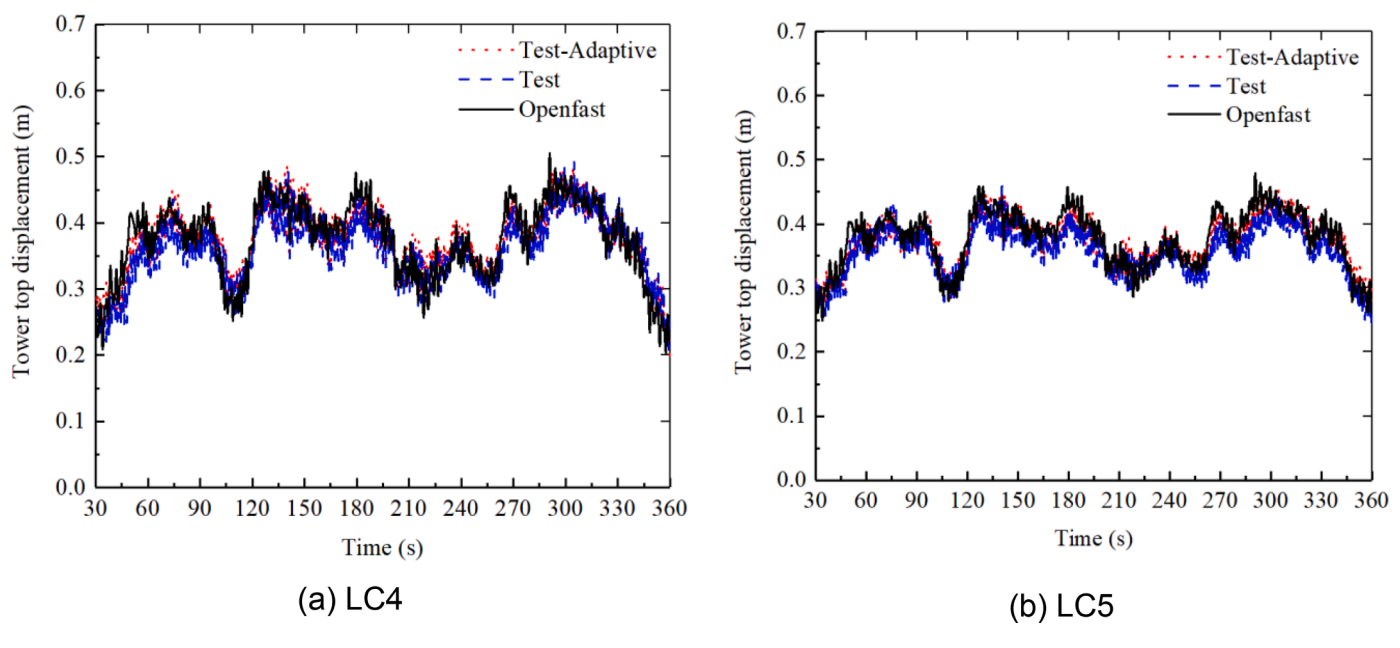


Fig. 14. Comparison of Tower top displacement time domain results between simulation and test.

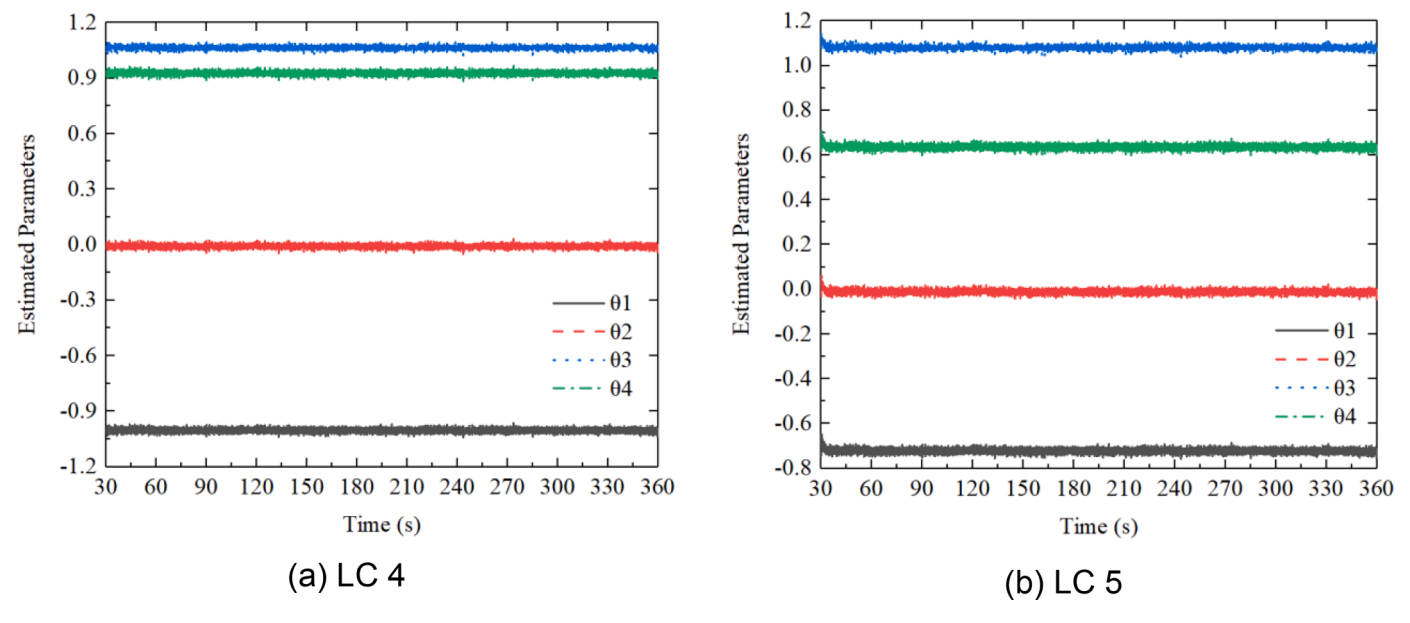


Fig. 15. Estimated parameters of the experimental process.

Table 7Performance indicators for RotThrust of simulation and test results under different turbulence intensity.

Object	Load case	Test Strategy	J1 (%)	J2(%)	J3 (%)
RotThrust	4	Test Test- Adaptive	5.61 -2.35	-10.75 -2.73	4.67 3.47
	5	Test Test- Adaptive	5.42 1.68	-9.79 -2.18	4.66 3.25
Tower top displacement	4	Test Test- Adaptive	13.08 5.42	-15.10 -7.29	7.89 6.76
	5	Test Test- Adaptive	12.43 4.89	-15.01 -5.74	6.80 4.79

editing. Huimeng Zhou: Writing - review & editing. Xin Li: Project administration.

Declaration of competing interest

The authors declare that they have no known competing financial interests or personal relationships that could have appeared to influence the work reported in this paper.

Data availability

Data will be made available on request.

Acknowledgment

This research was funded by the Key Technology Research and Development Program (2022YFB4201304). This paper is also partially funded by National Natural Science Foundation of China (Grant No. 52071058, 51939002, 52001052), the Natural Science Foundation of Guangdong Province (2022A1515010500) and the Guangzhou City School Joint Project (2023A03J0086). Madjid Karimirad would like to thank the support of a research grant from the Department for the Economy Northern Ireland under the US-Ireland R&D Partnership Programme.

References

- Azcona, J., Bouchotrouch, F., González, M., Garciandía, J., Munduate, X., Kelberlau, F., Nygaard, T.A., 2014. Aerodynamic thrust modelling in wave tank tests of offshore floating wind turbines using a ducted fan. In: Proceedings of the Journal of Physics: Conference Series, 524. IOP Publishing, 012089.
- Azcona, J., Bouchotrouch, F., Vittori, F., 2019. Low-frequency dynamics of a floating wind turbine in wave tank–scaled experiments with SiL hybrid method. Wind Energy 22 (10), 1402–1413.
- Bachynski, E.E., Chabaud, V., Sauder, T., 2015. Real-time hybrid model testing of floating wind turbines: sensitivity to limited actuation. Energy Procedia 80, 2–12.
- Bachynski, E.E., Thys, M., Sauder, T., Chabaud, V., Sæther, L.O., 2016. Real-time hybrid model testing of a braceless semi-submersible wind turbine: part II—experimental results. In: Proceedings of the International Conference on Offshore Mechanics and Arctic Engineering, 49972. American Society of Mechanical Engineers, V006T09A040.
- Berthelsen, P.A., Bachynski, E.E., Karimirad, M., Thys, M., 2016. Real-time hybrid model tests of a braceless semi-submersible wind turbine: part III—calibration of a numerical model. In: Proceedings of the International Conference on Offshore Mechanics and Arctic Engineering, 49972. American Society of Mechanical Engineers, V006T09A047.
- Bonnet, P., Lim, C., Williams, M., et al., 2007. Real-time hybrid experiments with newmark integration, MCSmd outer-loop control and multi-tasking strategies. Earthq. Eng. Struct. Dyn. 36 (1), 119–141.
- Cao, H., Bai, X., Ma, X., Yin, Q., X, Y., 2022. Numerical simulation of icing on Nrel 5-MW reference offshore wind turbine blades under different icing conditions. China Ocean Eng. 36 (5), 767–780.
- Cao, Y., Tahchiev, G., 2013. A study on an active hybrid decomposed mooring system for model testing in wave tank for offshore platforms. In: Proceedings of the ASME 2013 32nd International Conference on Ocean, Offshore and Arctic Engineering, 55317. American Society of Mechanical Engineers, V001T01A080.
- Chabaud, V., Steen, S., Skjetne, R., 2013. Real-time hybrid testing for marine structures: challenges and strategies. In: Proceedings of the International Conference on Offshore Mechanics and Arctic Engineering, 55393. American Society of Mechanical Engineers, V005T06A021.
- Chae, V., Kazemibidokhti, K., Ricles, J.M., 2013. Adaptive time series compensator for delay compensation of servo-hydraulic actuator systems for real-time hybrid simulation. Earthq. Eng. Struct. Dyn. 42 (11), 1697–1715.
- Chae, Y., Rabiee, R., Dursun, A., Kim, C.Y., 2018. Real-time force control for servo-hydraulic actuator systems using adaptive time series compensator and compliance springs. Earthq. Eng. Struct. Dyn. 47 (4), 854–871.
- Chen, M., Deng, J., Yang, Y., Zhou, H., Tao, T., Liu, S., Sun, L., Lin, H., 2024.
 Performance analysis of a floating wind-wave power generation platform based on the frequency domain model. J. Mar. Sci. Eng. 12 (2), 0206.
- Darby, A.P., Williams, M.S., Blakeborougha, 2002. Stability and delay compensation for real-time substructure testing. J. Eng. Mech. 128 (12), 1276–1284.
- DNV G L, 2016. Dnv gl-st-0437: Loads and Site Conditions For Wind Turbines. DNV GL, Oslo, Norway.
- Feng, J., Shen, W., 2017. Design optimization of offshore wind farms with multiple types of wind turbines. Appl. Energy 205, 1283–1297.
- Ferčák, O., Bossuyt, J., Ali, N., Cal, R.B., 2022. Decoupling wind-wave-wake interactions in a fixed-bottom offshore wind turbine. Appl. Energy 309, 118358.
- Fu, J., Shi, W., Wang, W., Li, X., Zhou, Y., 2023. Study on simulation of real-time hybrid model test for offshore wind turbines. Earthq. Eng. Resilience 2 (1), 94–110.
- Hall, M., Goupee, A., Jonkman, J., 2018. Development of performance specifications for hybrid modeling of floating wind turbines in wave basin tests. J. Ocean. Eng. Mar. Energy 4 (1), 1–23.
- Horiuchi, T., Inoue, M., Konno, T., Namita, Y., 1999. Real-time hybrid experimental system with actuator delay compensation and its application to a piping system with energy absorber. Earthq. Eng. Struct. Dyn. 28 (10), 1121–1141.
- Jonkman, B.J., 2014. TurbSim User's Guide v2. 00.00. National Renewable Energy Lab. Jonkman, J., Butterfield, S., Musial, W., Scott, G., 2009. Definition of a 5-MW Reference Wind Turbine For Offshore System Development. National Renewable Energy Lab, Golden, COUnited States.
- Jonkman, J.M., Buhl, M.L., 2005. FAST User's Guid. National Renewable Energy Laboratory, Golden, CO, USA.

- Ma, K., Zhao, Y., Zhao, Q., Xie, H., Li, J., 2024. Numerical simulations of fault stick–slip characteristics in different temperature fields at laboratory scale. Geomech. Geophys. Geo Energy Ge Resour. 10 (1), 1–22.
- Musial, W., Heimiller, D., Beiter, P., Scott, G., Draxl, C., 2016. 2016 Offshore Wind Energy Resource Assessment For the United States. National Renewable Energy Lab, Golden, COUnited States.
- Nakashima, M., Nagae, T., Enokida, R., Kajiwara, K., 2018. Experiences, accomplishments, lessons, and challenges of E-defense—tests using world's largest shaking table. Jpn. Architect. Rev. 1 (1), 4–17.
- Ning, X., Huang, W., Xu, G., Wang, Z., Wu, B., Zheng, L., Xu, B., 2023. A novel model-based adaptive feedforward-feedback control method for real-time hybrid simulation considering additive error model. Struct. Control Health Monit. 2023 (1), 5550580.
- Palacio-Betancur, A., Soto, M.G., 2019. Adaptive tracking control for real-time hybrid simulation of structures subjected to seismic loading. Mech. Syst. Signal. Process. 134, 106345.
- Pang, Z., Cui, H., 2009. Simulations of System Identification and Adaptive Control Using MATLAB. Beihang University Press, Beijing.
- Perveen, R., Kishor, N., Mohanty, S.R., 2014. Offshore wind farm development: present status and challenges. Renew. Sustain. Energy Rev. 29, 780–792.
- Phillips B.M., Spencer Jr B.F.. Model-based feedforward-feedback tracking control for real-time hybrid simulation. Newmark Structural Engineering Laboratory Report Series 028, 2011.
- Qin, M., Shi, W., Chai, W., Fu, X., Li, L., Li, X., 2023. Extreme structural response prediction and fatigue damage evaluation for large-scale monopile offshore wind turbines subject to typhoon conditions. Renew. Energy 208, 450–464.
- Ren, Y., Shi, W., Venugopal, V., Zhang, L., Li, X., 2024. Experimental study of tendon failure analysis for a TLP floating offshore wind turbine. Appl. Energy 358, 122633.
- Ren, Z., Han, X., Yu, X., Skjetne, L.B.J., Sævik, S., Zhu, M., 2023. Data-driven simultaneous identification of the 6DOF dynamic model and wave load for a ship in waves. Mech. Syst. Signal. Process. 184, 109422.
- Rui, Z., Zongji, C., 2009. Theory and Applications of Adaptive Technique-Control, Filter, Forecast. National Defence Industry Press, Beijing, p. 134–189.
- Sauder, T., Chabaud, V., Thys, M., Bachynski, E.E., Sæther, L.O., 2016. Real-time hybrid model testing of a braceless semi-submersible wind turbine: part I—the hybrid approach. In: Proceedings of the International Conference on Offshore Mechanics and Arctic Engineering, 49972. American Society of Mechanical Engineers, V006T09A039.
- Shi, W., Fu, J., Ren, Z., Jiang, Z., Wang, T., Cui, L., Li, X., 2023. Real-time hybrid model tests of floating offshore wind turbines: status, challenges, and future trends. Appl. Ocean Res. 141, 103796.
- Shi, W., Hu, L., Lin, Z., Zhang, L., Wu, J., Chai, W., 2023. Short-term motion prediction of floating offshore wind turbine based on muti-input LSTM neural network. Ocean Eng. 280, 114558.
- Shi, W., Yan, C., Ren, Z., Yuan, Z., Liu, Y., Zheng, S., Li, X., Han, X., 2024. Review on the development of marine floating photovoltaic systems. Ocean. Eng 286, 115560.
- Smith, A., Stehly, T., Musial, W., 2015. 2014-2015 Offshore Wind Technologies Market Report. National Renewable Energy Lab, Golden, COUnited States.
- Vilsen, S.A., Sauder, T., Føre, M., Sørensen, A.J., 2018. Controller analysis in real-time hybrid model testing of an offshore floating system. In: Proceedings of the International Conference on Offshore Mechanics and Arctic Engineering, 51272. American Society of Mechanical Engineers, V07BT06A024.
- Vilsen, S.A., Sauder, T., Sørensen, A.J., Føre, M., 2019. Method for real-time hybrid model testing of ocean structures: case study on horizontal mooring systems. Ocean Eng. 172, 46–58.
- Vilsen, S.A., Sauder, T., Sørensen, A.J., 2017. Real-time hybrid model testing of moored floating structures using nonlinear finite element simulations. In: Dynamics of Coupled Structures, 4. Springer, Cham, pp. 79–92.
- Wan, L., Moan, T., Gao, Z., Shi, W., 2024. A review on the technical development of combined wind and wave energy conversion systems. Energy 294, 130885.
- Wang, Z., Xu, G., Li, Q., Bin, W., 2020. An adaptive delay compensation method based on a discrete system model for real-time hybrid simulation. Smart. Struct. Syst. 25 (5), 569–580.
- Wu, B., Wang, Z., Bursi, O.S., 2013. Actuator dynamics compensation based on upper bound delay for real-time hybrid simulation. Earthq. Eng. Struct. Dyn. 42 (12), 1749–1765.
- Zeng, X., Shi, W., Michailides, C., Wang, K., Li, X., 2021. Comparative experimental and numerical study of wave loads on a monopile structure using different turbulence models. China Ocean Eng. 35, 554–565.
- Zeng, X., Shi, W., Michailides, C., Zhang, S., Li, X., 2021. Numerical and experimental investigation of breaking wave forces on a monopile-type offshore wind turbine. Renew. Energy 175, 501–509.
- Zhai, Y., Zhao, H., Li, X., Feng, M., Zhou, Y., 2024. Effects of aquaculture cage and netting on dynamic responses of novel 10 MW barge-type floating offshore wind turbine. Ocean Eng. 295, 116896.
- Zhang, L., Li, Y., Xu, W., Gao, Z., Fang, L., Li, R., He, F., 2022. Systematic analysis of performance and cost of two floating offshore wind turbines with significant interactions. Appl. Energy 321, 119341.
- Zhang, S., Mu, C., Feng, X., Ma, K., Guo, X., Zhang, X., 2024. Intelligent dynamic warning method of rockburst risk and level based on recurrent neural network. Rock. Mech. Rock. Eng. 57, 3509–3529.
- Zhao, H., Hu, Y., Bi, C., Li, X., 2024. Numerical study on hydrodynamic behaviors of and flow field around UHMWPE plane nets. Aquac. Eng. 106, 102397.
- Zhao, Y., She, X., He, Y., Yang, J., Peng, T., Kou, Y., 2018. Experimental study on new multi-column tension-leg-type floating wind turbine. China Ocean Eng. 32, 123–131.